Desalination and Water Treatment
www.deswater.com

doi: 10.5004/dwt.2020.24840

174 (2020) 344–353
January

In_2O_3 catalyst supported on carbonaceous nanohybrid for enhancing the removal of methyl orange dye from aqueous solutions

Sahar M. El-Khouly[a], Nady A. Fathy[a,*], Hala K. Farag[b], Reham M.M. Aboelenin[a]

[a]*Physical Chemistry Department, National Research Centre, 33 El Bohouth Street (Former Tahrir Street), P.O. Box: 12622, Dokki, Giza, Egypt, Tel. +20 2 33371433; Fax +20 2 33370597; emails: fathyna.77@hotmail.com (N.A. Fathy), sm_elkhouly@yahoo.com (S.M. El-Khouly), reham_aboelenin@yahoo.com (R.M.M. Aboelenin)*
[b]*Inorganic Chemistry Department, National Research Centre, 33 El Bohouth Street (Former Tahrir Street), P.O. Box: 12622, Dokki, Giza, Egypt, email: msherif888@yahoo.com*

Received 1 May 2019; Accepted 29 August 2019

ABSTRACT

This work aims to assess the adsorption and catalytic wet oxidation (CWO) performance of In_2O_3 supported on carbonaceous nanohybrid (In_2O_3-CNH). CNH was prepared from carbon xerogel reinforced with graphene oxide through sol-gel of resorcinol–formaldehyde then followed by carbonization at 500°C for 2 h. The morphological, chemical and textural properties of nanohybrids obtained were determined using scanning electron microscopy/energy-dispersive X-ray spectroscopy, X-ray diffraction, Fourier transform infrared spectroscopy and N_2 gas adsorption at –196°C measurements. The adsorption efficiency of CNH and In_2O_3-CNH samples toward methyl orange dye (MO) was studied. CWO experiments over the In_2O_3-CNH catalyst were performed at different variables like the temperature, pH of the solution and initial dye concentrations. The reusability of the nanohybrid catalyst was employed also. Adsorption results showed that In_2O_3-CNH possesses larger adsorption capacity (58.8 mg/g) than that of CNH (32.2 mg/g). The most effective catalytic oxidation performance of In_2O_3-CNH was attained at a temperature of 40°C, pH 4 and initial MO concentration of 20 mg/L to degrade fully the dye within 30 min. Results of reusability showed excellent catalytic performance for In_2O_3-CNH during four CWO cycles, indicating superior degradation toward MO dye up to 88% till 180 min at the fourth CWO run. Overall, the obtained In_2O_3-CNH has higher adsorptive and catalytic activity than that of CNH individually, confirming that In_2O_3 nanoparticles played a key role as reactive sites at the surface of CNH.

Keywords: Carbonaceous nanohybrid; Indium oxide; Methyl orange dye; Adsorption; Catalytic wet oxidation

1. Introduction

Dyes discharged in the industrial wastewater have an unfavorable impact on the environment because they are considered as toxic substances. Also, they have carcinogenic properties, which make the water inhibitory to aquatic life. During the dyeing and finishing operations in the textile industry, more than 20,0000 tones of dyes are lost to effluents annually because of the inefficiency of dyeing processes [1]. There are various techniques for dye removal and classified into physical, biological and chemical methods [1–4]. Physical methods include adsorption, ion exchange, and filtration/coagulation methods, etc. Biological methods include aerobic degradation, anaerobic degradation, biosorption, etc. While chemical methods include electrocatalytic oxidation, Fenton oxidation, and photocatalytic oxidation which known as advanced oxidation processes (AOPs). However, when the wastewater contains large concentrations of various dyes;

* Corresponding author.

the remediation of wastewater using physical and biological methods became more difficult and expensive. Nevertheless, AOPs lately emerge as the most promising technology for the remediation of concentrated dyes in the contaminated water on a large scale. AOPs were firstly proposed in the 1980 s for potable water treatment. Such processes involve the formation of hydroxyl radicals ($HO^{\bullet}$) in sufficient quantity using oxidizing agents such as H_2O_2 and O_3 [5,6].

In particular, heterogeneous catalytic wet oxidation process (CWO) using H_2O_2 in the presence of a metal catalyst supported on carbon materials is recognized as an effective technology for treating wastewater polluted with various refractory organic compounds [7–15]. As well, the contribution of oxygen-, nitrogen-, sulfur- and phosphorous-containing surface groups into the surface composition of carbon materials could enhance their catalytic performance of carbons through CWO processes [4,8,16]. In our recent studies, composites of zero-valent metals such as Ni/carbon xerogels [11], metal oxides such as MnO_2/carbon nanotubes [9,12], ZnO or CeO_2/activated carbons [13], Fe_2O_3 or Ag_2O-Fe_2O_3/carbon nanotubes [14] and CeO_2/carbon xerogels [15] were prepared and investigated in removing the synthetic dyes from their aqueous solutions. Furthermore, the CWO performance of carbon xerogel doped by P- and N-elements was studied as metal-free catalysts for the degradation of 4-nitrophenol from the aqueous solutions [16]. Consequently, a beneficial CWO activity could be obtained by introducing the catalysts into the carbon matrix.

Owing to its high electrical conductivity, high charge-carrier mobility, and transparency in the visible region, indium oxide (In_2O_3) as an *n*-type semiconductor is versatile and relevant for numerous applications including solar cells, organic light-emitting diodes, optoelectronics, photocatalysts, field emission, architectural glasses and gas sensors [17–21]. Several synthesis techniques were employed for fabricating In_2O_3 nanostructures include chemical vapor deposition, hydrothermal, sol–gel, and electrodeposition routes, which may require high calcination temperature (up to 1,300°C) [22–25]. Of late, In_2O_3 nanostructures with different morphologies such as nanorods, nanocubes, nanospheres, nanoplates, nanorhombohedral and flowers were synthesized [22–26]. Recent reports have shown that both the morphology and electronic defect structure of In_2O_3 affect strongly its catalytic, gas sensing and photo-electrochemical properties [21,22,26]. However, substantial efforts made to improve the structural stability and enhance the catalytic performance of In_2O_3 by mixing with carbon materials to prepare nanostructure hybrids. For example, carbon nanotubes [27], graphene [28–30], graphene oxide (GO) [31], graphitic carbon nitride (C_3N_4) [32] and carbon nanofiber [33] were encapsulated by In_2O_3 for applying as gas sensor, photocatalyst, and lithium-ion storage.

More recently, resorcinol–formaldehyde/GO carbonaceous nanohybrids (CNHs) of a three-dimensional structure have attracted enormous interest because of their unique electronic property, flexible structure, high electrical conductivity, excellent adsorptive as well as large specific surface area [34–39]. This hybrid was prepared by adding GO through a sol-gel polymerization of resorcinol with formaldehyde in basic or acidic medium, drying of the organic gels, and subsequent carbonization process at high temperature in an inert gas atmosphere [38,39]. The presence of GO was found to be the strength of the nanostructure and suppress the collapse of nanopores of resorcinol–formaldehyde (RF) aerogels during the drying process [34]. Accordingly, to the author's knowledge, the synthesis of In_2O_3 supported on CNH consisting of carbon xerogel reinforced with GO, as a catalyst for the decomposition of the methyl orange (MO) dye in the liquid phase; has not been published yet.

Therefore, the main objective of this paper is to address the adsorption and catalytic efficiency of In_2O_3-CNH with comparison to the individual CNH sample in the CWO processes for removing MO dye from their aqueous solutions. The morphology, chemical and porosity properties of the as-prepared nanohybrids were analyzed. The effect of various factors such as temperature, pH and initial concentrations of MO dye were investigated. The reusability of the nanohybrid catalyst through four cycles of CWO has studied also.

2. Materials and methods

2.1. Materials and reagents

Commercial graphite powder (99.9%, <45 μm) and (MO, $C_{14}H_{14}N_3NaO_3S$) were purchased from Sigma-Aldrich (Germany). Orthophosphoric acid (H_3PO_4, 85%) and hydrogen peroxide (30%) were supplied from Rasayan, (Turkey). Potassium permanganate ($KMnO_4$, 99%) and sodium carbonate (Na_2CO_3, 99%) were obtained from POCH SA, (Poland). Formaldehyde solution (HCHO, 36%–38%), methanol (CH_3OH, 99%), sulfuric acid (H_2SO_4, 95%–98%), nitric acid (HNO_3, 68%) and hydrochloric acid (HCl, 37%) were purchased from Adwic Co., Egypt. Resorcinol ($C_6H_4(OH)_2$, 99%) and sodium hydroxide (NaOH, 98%) were obtained from Panreac Química S.A., Spain.

The ionic liquid 1-ethyl-3-methylimidazolium trifluoromethyl sulfonate ([EMIm] TFO) with purity 99% (Io.Li.Tec., Germany) was employed. Indium chloride (Aldrich, 99.99%) was used as a precursor for the synthesis of In_2O_3. Isopropanol (99.5%, Alfa Aesar, India) was used for washing the obtained oxides to remove the trapped ionic liquids. Ammonium hydroxide (98%, Sigma-Aldrich, Germany) was used to adjust the pH. All the reagents were used as received without further purification. Double distilled water used throughout this work.

2.2. Synthesis of GO

According to modified Hummer's method that published in [40,41], GO was prepared as follows: 0.75 g of graphite fakes was dispersed in 9:1 mixture of H_2SO_4 and H_3PO_4 in an ice bath under stirring for 30 min. Then, 4.5 g of $KMnO_4$ was slowly added under stirring for 30 min. After that, the temperature was gradually raised to 50°C. The reaction vessel was kept at this temperature for 12 h under constant stirring. The colloidal mixtures were transferred into a beaker containing 30 mL H_2O_2 and 200 mL cooled water and slowly stirred for a few minutes. The obtained brilliant yellow precipitate was centrifuged, filtered, washed with 10% HCl solution, water, and ethanol respectively till pH of 5 and then dried in an air-oven at 50°C for 72 h.

2.3. Synthesis of CNH

The CNH was prepared during the sol-gel of resorcinol (R) and formaldehyde (F) in the presence of (RF/GO) as described in [34] and followed by the carbonization. The sol-gel procedure was carried out by adding reactants of R, Na_2CO_3 as alkaline catalyst (C) to 1 wt.% GO dispersed in 10 mL distilled water (W). Then, the formaldehyde solution (F) stabilized by 10% methanol was slowly added into this mixture under vigorous stirring to form the hydrogel. The hydrogel was obtained after 30 min at 80°C. The molar ratios of the used reactants with respect to resorcinol were calculated as; R/F = 0.5, R/C = 500 and R/W = 0.027. The pH of the sol was adjusted to 6 by 0.1 M NaOH solution. The prepared hydrogel was then transferred into a stoppered glass bottle and heated in an air-oven at 80°C for 24 h to complete the curing and gelling process. Afterward, the sealed bottle was opened to allow the gel obtained for drying at the same temperature for another 48 h. to form brownish-black monolithic gels. In a vertical tubular reactor, the pyrolysis of the dried nanohybrid gel was carried out at 500°C under passing N_2 gas for 2 h and the product was labeled as CNH.

2.4. Synthesis of In_2O_3 nanoparticles

The ultrasonic-assisted synthesis of In_2O_3 was performed using an ordinary ultrasonic cleaner (S 120 H Elmasonic, Germany) with an operating frequency of 37 kHz. The pH was adjusted at 9 by a dropwise addition of NH_4OH. After that, the mixtures were centrifuged to regain the product and washed with water several times. The sample was dried at 70°C and calcined in a muffle oven at 500°C for 5 h to ensure getting rid of the ionic liquid residues. After cooling, the obtained oxide was washed with ethanol and then dried.

2.5. Preparation of In_2O_3 supported on CNH

In_2O_3 was prepared on the surface of CNH by sonochemical of dissolved $InCl_3$ in the ionic liquid of ([EMIm](TFO) over (RF/GO) precursor then followed by the calcination process. The sonochemical method was carried out according to the described methods elsewhere [42,43]. A mixture solution of $InCl_3$, ([EMIm](TFO) and RF/GO precursor was prepared with a mass ratio of 1 $InCl_3$: 10 RF/GO and kept under stirring at 60°C for several hours till the solution became homogeneous. Then a sonication was applied and the pH was adjusted to be 9 by NH_4OH. After filtration, the solid sample was dried at 100°C overnight. Then, the dried sample was calcined in a vertical tubular reactor at 500°C under N_2 atmosphere for 2 h and the product was labeled as In_2O_3-CNH.

2.6. Characterization of the materials

Various techniques were employed for the characterization of the obtained materials. The morphology and chemical composition analyses of the samples were estimated by field emission-scanning electron microscope combined with energy-dispersive X-ray spectroscopy and electron backscatter diffraction (HR-SEM, FEI Quanta FEG-250, EDX, Japan). The structure of the prepared In_2O_3-CNH sample was analyzed by High-resolution transmission electron microscopy (HR-TEM, JEM-1230, Japan). An X-ray diffractometer with CuKα radiation and graphite monochromator (PW-2103, Philips, Japan) was used to investigate the main crystalline phases. X-ray diffraction patterns (XRD) were run with Ni-filtered copper radiation (λ = 1.5418 Å) at 35 kV and 20 mA, and a scanning speed of 2° in 20 min^{-1}. The main functional surface groups of the prepared samples were determined by Fourier-transform infrared (FTIR) spectroscopy using KBr pellets JASCO, FT-IR 460 plus, (USA). The principal textural properties such as the specific surface area (m^2/g), total pore volume (cm^3/g) and average pore diameter (Å) were determined using nitrogen adsorption analysis at –196°C (BEL-Sorp, Microtrac Bel Crop, Japan).

2.7. Adsorption studies and isotherm models

To estimate the adsorption efficiency of the prepared CNHs, the adsorption experiments were performed onto CNH and In_2O_3-CNH samples. In a typical, 25 mg of catalyst was conducted in 25 mL of MO dye initial concentrations ranged from 20 to 200 mg/L under shaking for 24 h at both initial pHs of dye (5.5) and 25°C.

Langmuir, Freundlich, and Temkin isotherm models [44–46] were applied to explore the adsorption capacity of the prepared samples. Equations and constants of these models are listed in Table 1.

2.8. CWO experiments

CWO experiments were carried out in a 250 mL glass-round bottle reactor equipped with a condenser placed on a heater with a magnetic stirrer (200 rpm). Before catalytic oxidation experiments, the mixture solution containing catalyst and MO dye was magnetically stirred in absence of H_2O_2 for 30 min at room temperature to attain the adsorption-desorption equilibrium between MO dye and catalysts to ensure that the removal of this dye was done by catalytic oxidation only. By conducting 50 mg of tested sample with 50 mL of MO dye (20 mg/L) and 1 mL H_2O_2 (0.192 mol/L), the effect of temperature on the catalytic activity of catalyst at 25°C, 40°C and 60°C as well as the effect of pH at 2, 4, 6 and 8 were studied during interval times of 0–180 min. The pH was adjusted using 0.1 mol/L H_2SO_4 or NaOH solutions. The influence of initial MO dye concentrations of 20–200 mg/L on the catalytic oxidation performance of the In_2O_3-CNH catalyst was investigated at pH 4 and 40°C under fixing the other parameters.

The residual concentration of MO dye in the solution either by catalytic wet peroxide oxidation or adsorption was determined using a double beam UV-Vis spectrophotometer (Shimadzu-2401 PC, Japan) at 465 nm to calculate the percent removal (%R) and/or catalytic decomposition rate (C_t/C_0). About two drops from a sodium thiosulfate solution (0.1 mol/L) was added to the aliquot solution to stop the CWO reaction. To separate the solid phase and avoid possible interferences, all samples were subjected to centrifugation at 1,000 rpm during 5 min before analysis. To assess the reproducibility and error of the CWO tests, the absorbance of dye was measured in triplicate, and the results showed that the relative errors were lower than ±3%.

Table 1
Adsorption isotherm models used to describe the adsorption of MO dye using the obtained samples

Models	Equations	Parameters	References
Langmuir	$\frac{C_e}{q_e}=\frac{1}{K_L Q}+\frac{1}{Q}C_e$	C_e is the equilibrium concentration of MO dye (mg/L), q_e the adsorbed amount of MO dye at equilibrium (mg/g), and Q is the maximum monolayer adsorption (mg/g) and K_L (L/g) is the Langmuir adsorption equilibrium constant. Q and K_L are calculated from the slope and intercept of the isotherm plot C_e/q_e vs. C_e.	[44]
Freundlich	$\log q_e=\log K_F+\frac{1}{n}\log C_e$	K_F (mg/g(L/mg)$^{1/n}$) is roughly an indicator of the adsorption capacity and $1/n$ is the adsorption intensity. Freundlich constants K_F and $1/n$ can be calculated from the intercept and slope of the linear plot derived from log q_e vs. log C_e.	[45]
Temkin	$q_e=B_1\log K_T+B_1\log C_e$	$B_1 = (RT/b)$ and K_T are the Temkin constants. R is universal gas constant = 8.314 J/mol K, and T is absolute temperature (K). K_T is the equilibrium binding constant (L/mol) corresponding to the maximum binding energy, b is the variation of adsorption energy (J/mol) and constant B_1 is related to the heat of adsorption. B_1 and K_T values can be obtained from the slope and intercept of linear plot for plotting log C_e vs. q_e.	[46]

2.9. Reusability cycles

In order to estimate the utilization of catalyst through CWO technique, four consecutive experiments of CWO for MO dye using the catalyst of In_2O_3-CNH were performed under the operating conditions: 50 mL of [MO] = 20 mg/L, 1 mL of [H_2O_2] = 0.192 mol/L, [In_2O_3-CNH] = 1 g/L, T = 40°C, reaction time = 0–180 min and pH = 4. After each run, the selected catalyst was filtered, washed thoroughly with hot distilled water and dried at 80°C overnight and then reused with a fresh concentration of MO dye solution (20 mg/L).

3. Results and discussion

3.1. Scanning electron microscopy, TEM and EDX examinations

Morphologies related to the prepared samples of In_2O_3, CNH and In_2O_3-CNH were determined using scanning electron microscopy (SEM). SEM image of In_2O_3 reveals that In_2O_3 nanoparticles are relatively aggregated like cubic-shape (Fig. 1a). The morphology of the CNH sample showed nodules of carbon spheres reinforced with graphene plates as shown in Fig. 1b. The surface of the In_2O_3-CNH sample is almost covered by In_2O_3 nanoparticles (Fig. 1c). Also, a representative TEM image of In_2O_3-CNH is given in Fig. 1d, exhibiting the size of In_2O_3 nanoparticles is approximately ranged from 3.8 to 43 nm.

Furthermore, the surface chemical compositions are demonstrated using EDX combined with an SEM device. Table 2 lists the weight percentage of each element in RF resin/GO nanohybrid and In_2O_3-CNH samples. The results affirmed the presence of C and O elements in larger amounts than N and In elements. The reduction in oxygen is probably due to the conversion of GO to reduced GO during calcination of RF resin/GO nanohybrid loaded with indium chloride at 500°C.

As shown in Table 2, the calculated textural parameters revealed that both nanohybrid samples possess good surface area and mesoporous character (pore width~ 6–8 nm). It is noted that the specific surface area and mesoporosity are considerably decreased after loading In_2O_3 nanoparticles on the surface of CNH. This result is probably attributed to the accommodation of In_2O_3 nanoparticles inside the internal pores of CNH structure.

3.2. XRD analysis

To investigate the crystalline phases of indium oxide formed in this study, XRD patterns of the control sample (In_2O_3) and In_2O_3 loaded on the carbon nanohybrid (In_2O_3-CNH) are depicted in Fig. 2. For pure In_2O_3 sample, their XRD peaks located at 2θ of 21.6°, 30.6°, 35.5°, 45.7°, 51.1°, and 61.2° are indexed to the cubic phase of In_2O_3 according to JCPDS No. 06-0416 [18,26]. This result is consistent with the SEM results. The crystallite size of the crystal phases was calculated according to the Scherrer equation of $d = K\lambda/\beta\cos\theta$. It was found that their sizes varied from 3.5 to 47.9 nm. It can be seen that the XRD patterns of In_2O_3 are almost identical to that of the In_2O_3-CNH sample with increasing in their intensity and shifting at 2θ values. This confirms the interaction between In_2O_3 and CNH samples.

3.3. FTIR spectra

Fig. 3 illustrates the main functional oxygen groups of $InCl_3$-RF/GO precursor and its corresponding carbonized sample (In_2O_3-CNH) at 500°C. Absorption bands in both FTIR spectra are relatively similar with considerable differentiates in their intensity. Oxygen-containing functional groups such as O–H (3,430–3,450 cm^{-1}), C=O (1,740 cm^{-1}), C–O–C (1,300–1,100 cm^{-1}) and C–O (1,050 cm^{-1}) are observed [31]. The absorption band at 1,620–1,640 cm^{-1} could be attributed to C=C skeleton vibration [37,47]. The bands at 2,925 and 2,857 cm^{-1} are signified to symmetric and asymmetric CH_2 and CH stretching vibrations in the aromatic ring. However, a reduction in the intensity of absorption bands related to the oxygen-containing functional groups is found after thermal treatment. This finding results from the reduction of GO to reduced GO in the obtained nanohybrid. In addition,

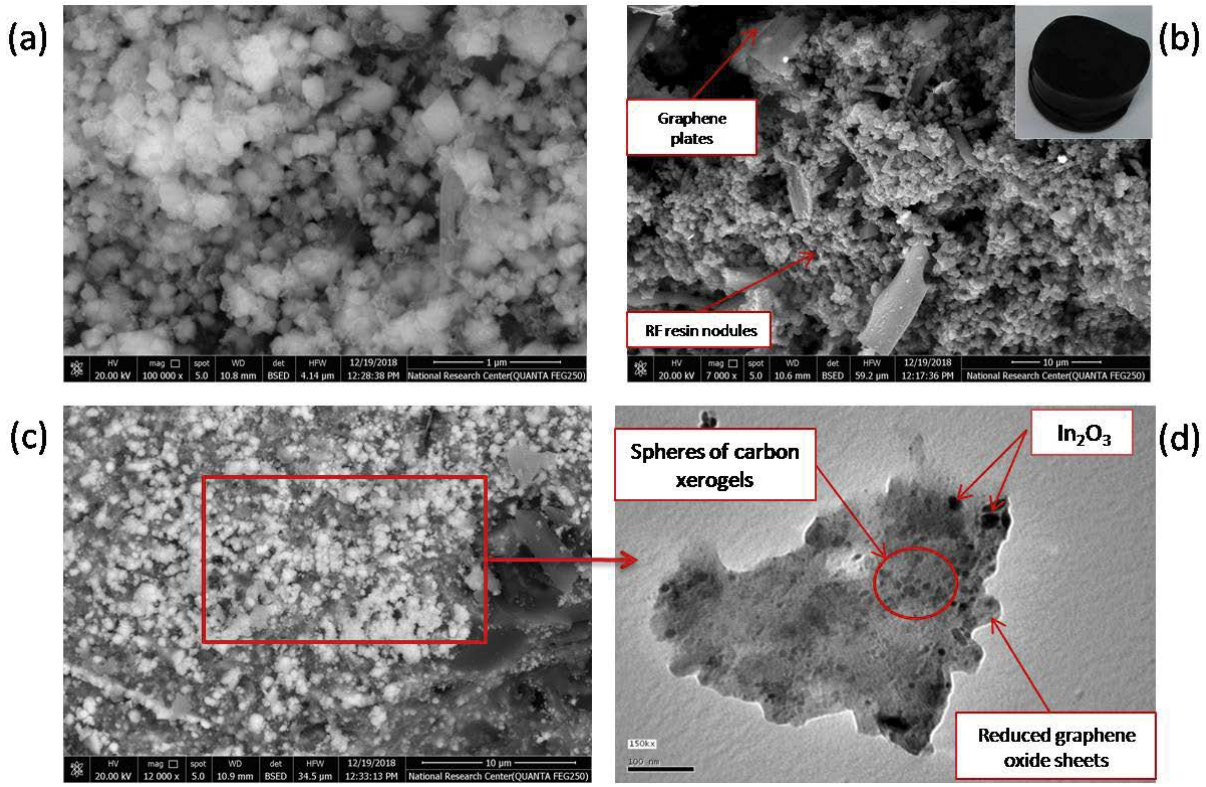

Fig. 1. SEM images of (a) In_2O_3 nanoparticles, (b) CNH with its corresponding gel mold, (c) In_2O_3-CNH, and (d) TEM image of In_2O_3-CNH.

the absorption bands related to In–O–C in the In_2O_3-CNH sample are detected between 600 and 425 cm^{-1} as reported previously [27–31].

According to the above results, thus In_2O_3-CNH sample was successfully obtained. In order to figure out the positive combination between CNH and In_2O_3 in improving the adsorption and catalytic oxidation properties of In_2O_3-CNH catalyst, the adsorption and CWO studies of MO dye using CNH and In_2O_3-CNH were determined.

3.4. Adsorption studies

To discriminate the adsorption performance of CNH and In_2O_3-CNH samples, different initial concentrations of MO dye (20–200 mg/L) were performed to determine the removal percentage (%) after 24 h. The results are shown in Fig. 4. Even though of its high specific surface area, CNH exhibits lower removal efficiency than that of In_2O_3-CNH. This means that the presence of In_2O_3 nanoparticles remarkably enhanced the adsorption performance of the obtained CNH. The maximum removal of MO dye (20 mg/L) is reached to 40% and 69% over CNH, and In_2O_3-CNH samples, respectively. The removal rate of dye is substantially decreased with increasing initial dye concentration, and hence at larger concentrations, there are insufficient adsorption sites.

To analyze the adsorption isotherms as shown in Fig. 5, three adsorption isotherm models were used and their calculated parameters are summarized in Table 3. The fitness degree of the linear curve derived from these models was examined by the calculation of regression coefficients (R^2). It was found that Langmuir and Temkin's models are more fitted to describe the adsorption of MO dye molecules by CNH and In_2O_3-CNH samples. As well, the values of monolayer adsorption capacity (Q, mg/g) and the variation of adsorption energy (b, J/mol) for removing MO dye by In_2O_3-CNH are larger than that obtained by CNH. Thus, the adsorption of MO dye is largely associated with the presence of In_2O_3 nanoparticles. This affirms the efficiency of In_2O_3 nanoparticles which can act as effective adsorption sites for removing MO dye from aqueous solutions when supported on CNH.

Table 2
Surface and textural properties of the prepared samples

Analysis	CNH	In_2O_3-CNH
pH	4.5	5.5
EDX (Weight %)		
C	66.2	70.2
O	33.1	20.8
N	0.70	1.7
In	0	7.3
N_2 adsorption		
Specific surface area (m^2/g)	139.3	128.1
Total pore volume (cm^3/g)	0.404	0.227
Average pore diameter (Å)	11.6	7.09
BJH mesopore width (nm)	8.34	6.44

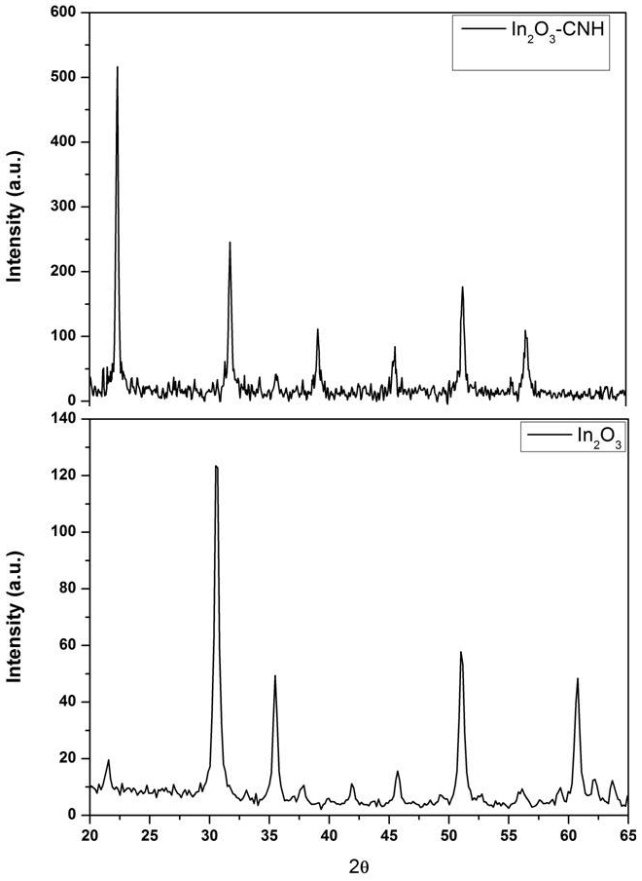

Fig. 2. XRD patterns of the prepared samples.

From the adsorption results, it is essential to remove completely the dye from the contaminated wastewater. Thus CWO processes using hydrogen peroxide in presence In_2O_3-CNH as a catalyst were carried out by varying the temperature, pH and initial MO dye concentrations at a constant catalyst dose of 1 g/L as shown in the next sections.

3.5. CWO studies

3.5.1. Effect of temperature

The influence of temperature on the catalytic activity of the In_2O_3-CNH catalyst was studied at 25°C, 40°C and 60°C for decomposing 20 mg/L of MO dye in the presence of H_2O_2 at pH 4. Fig. 6 shows the removal efficiency (%) results of MO dye as a function of contact time and temperature. It is seen that the highest temperature enhances the catalytic activity of this catalyst to decompose quickly the MO dye at 10 min. While at 25°C and 40°C the full decomposition of dye is happened at 150 and 30 min, respectively. Also, at another further temperature of 80°C, the dye is completely removed within 30 s (not shown here). As reported previously, the high temperature accelerated the decomposition rate of H_2O_2 to hydroxyl radicals ($HO^{\bullet}$) over the surface of catalyst resulting in an enhancement in the mobility of MO and H_2O_2 molecules from bulk solution toward the surface of the catalyst. Then, the formed $HO^{\bullet}$ radicals attack and crack the azo group (e.g. –N=N–) in the ring of dye and form

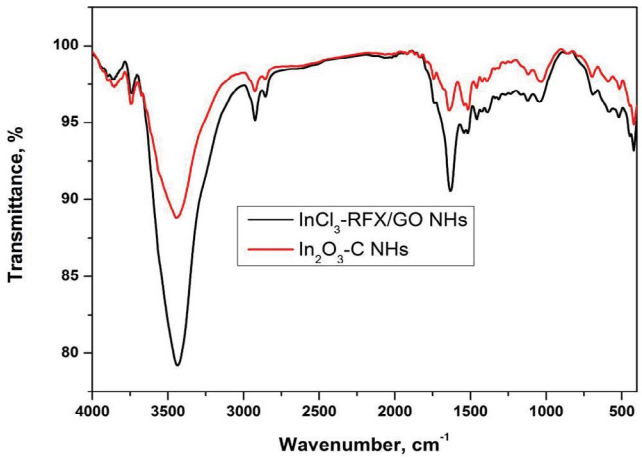

Fig. 3. FTIR spectra of the prepared samples.

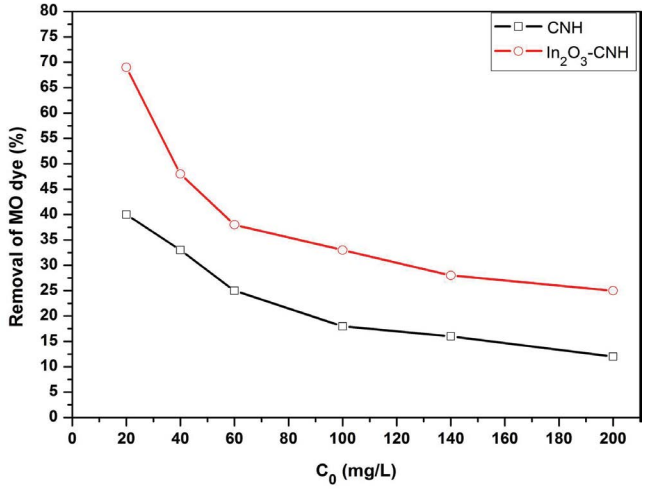

Fig. 4. Adsorption efficiency of CNH and In_2O_3-CNH samples towards the removal of MO dye at 25°C, catalyst dose = 1 g/L, contact time = 24 h and initial pH of dye = 5.5.

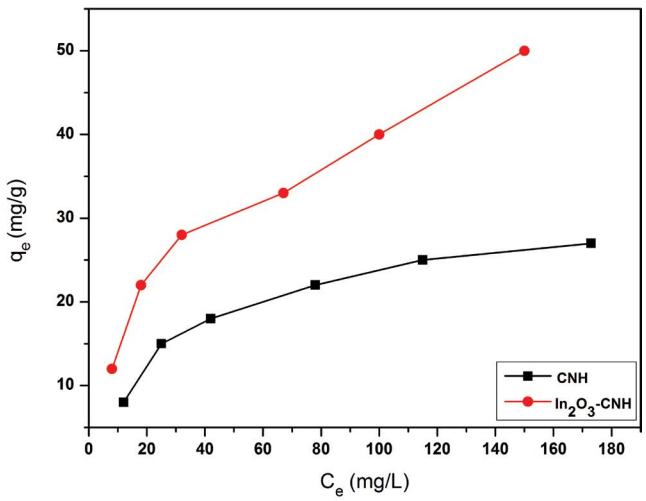

Fig. 5. Adsorption isotherms of MO dye onto the prepared adsorbents at 25°C and pH 5.5.

Table 3
Adsorption parameters calculated from Langmuir, Freundlich, and Temkin models

Equilibrium models	Adsorbents	
	CNH	In_2O_3-CNH
Langmuir		
Q (mg/g)	32.2	58.8
K_L (L/mg)	0.0300	0.0276
R^2	0.998	0.966
Freundlich		
K_F (mg/g (L/mg)$^{1/n}$)	3.22	5.36
$1/n$	0.432	0.446
R^2	0.928	0.963
Temkin		
b (J/mol)	90.5	153.4
K_T (L/mol)	0.880	0.328
R^2	0.990	0.965

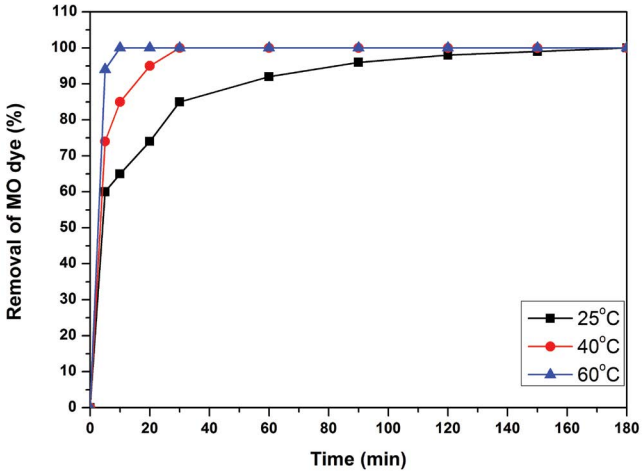

Fig. 6. Impact of temperature on the catalytic performance of In_2O_3-CNH catalyst (C_0 = 20 mg/L, catalyst dose = 1 g/L, pH = 4 and $[H_2O_2]$ = 0.192 mol/L).

several intermediates (e.g. benzene ring, phenol ring and so on) which converted to CO_2 and H_2O upon further attack by hydroxyl radicals [11,12,48].

At 5 min, it is found that more than 50% of the MO dye is decomposed by the In_2O_3-CNH catalyst at the studied temperatures. Thus such catalysts can be used effectively for removing the dye over a wide range of temperatures. Accordingly, the following catalytic oxidation experiments were performed at 40°C as a moderate temperature.

3.5.2. Effect of pH

In this respect, the effect of pH on the removal of MO dye with regarding the catalytic activity of the catalyst was studied at different values ranging from 2 to 8 as shown in Fig. 7. Other effective parameters such as catalyst loading (1 g/L), contact time (60 min) and temperature (40°C) were kept constant. The degradation efficiency of MO dye

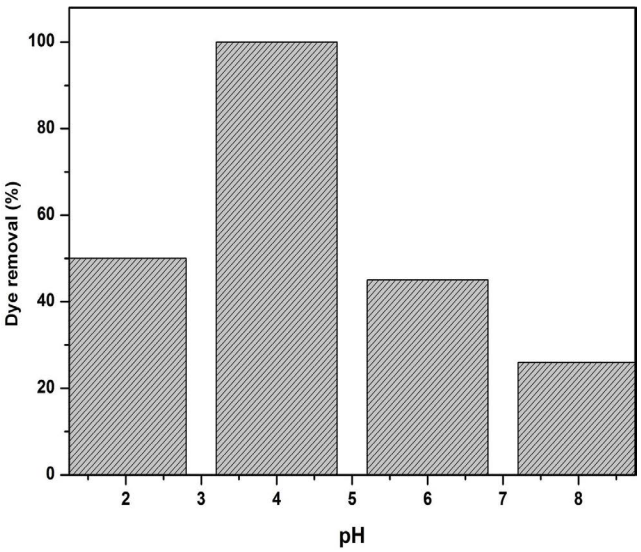

Fig. 7. Effect of pH on the degradation of MO dye over In_2O_3-CNH catalyst (C_0 = 20 mg/L, catalyst dose = 1 g/L, T = 40°C, $[H_2O_2]$ = 0.192 mol/L and contact time = 60 min).

increased sharply as pH increased from 2 to 4 and then decreased gradually at alkaline media. Thus the degradation of MO is considerably based on pH. This may be informed that the decomposition of H_2O_2 to hydroxyl radicals (HO•) over the surface of catalyst is produced little at the basic pH. Successively, the best removal efficiency of MO dye from aqueous solution using In_2O_3-CNH catalyst/H_2O_2 was found at pH 4. Since the dissociation constant (pK_a) of MO is 3.48, the MO dye is converted to quinoid form (anionic azo) at acidic pH which is easily degraded via HO• radicals [49]. At low acidic pH 2, the HO• radicals are partially trapped by excessive amount of H^+ ions forming $H_3O_2^+$, which increases the stability of H_2O_2 and suppresses the production of HO• radicals [50]. Also, the results are in accordance with other previous studies [51,52].

3.5.3. Effect of initial dye concentration

The influence of initial MO dye concentrations of 20–200 mg/L on the catalytic oxidation performance of the In_2O_3-CNH catalyst was studied under fixing the other parameters. As shown in Fig. 8, with increasing initial concentration from 20 to 200 mg/L, the degradation efficiency of dye is decreased. Catalytic oxidation performance of the In_2O_3-CNH catalyst showed a full degradation of MO dye at 30 and 120 min for 20 and 50 mg/L, respectively. Over 50 mg/L of MO dye, the degradation of dye is decreased to 98% for 100 mg/L and 90% for 200 mg/L at 180 min. This result may be ascribed to the occupation of all active sites by MO dye during the early reaction time. However, this notifies that the obtained nanohybrid catalyst has a superior performance to degrade MO dye at higher concentrations also. This may affirm that In_2O_3 formed accessible and active sites at the surface of the In_2O_3-CNH catalyst that responsible for adsorption of MO dye and generation of HO• radicals giving rise to an enhancement in the catalytic oxidation efficiency of CNH nanohybrid [11,48].

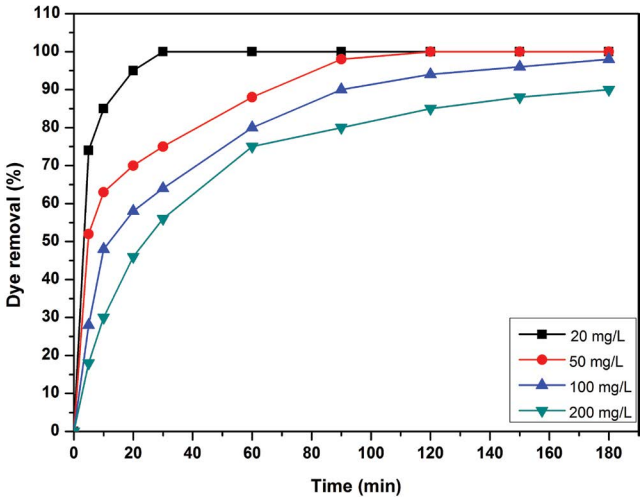

Fig. 8. Effect of MO dye concentration on the catalytic oxidation performance of In_2O_3-CNH catalyst (catalyst dose = 1 g/L, T = 40°C, pH = 4 and $[H_2O_2]$ = 0.192 mol/L).

3.5.4. Catalyst performance and stability studies

To state the catalytic oxidation efficiency of In_2O_3 supported on CNH, a comparison catalytic oxidation experiments on MO dye with H_2O_2 alone, CNH/H_2O_2 and In_2O_3-CNH/H_2O_2 as depicted in Fig. 9. It can be seen that the degradation rate of the MO dye is very slow when H_2O_2 is used only. This may be due to the negligible formation of HO• radicals. In the case of CNH/H_2O_2, the degradation rate (C/C_0) is increased slightly to reach 0.55 (i.e., 45% of dye removal) at 180 min. It can be suggested that the increase in degradation rate is due to the adsorption of MO molecules on the active sites of the CHN catalyst. Comparing to the results in Fig. 4, the adsorption efficiency of this sample is reached to 40% for treating 20 mg/L of MO after 24 h.

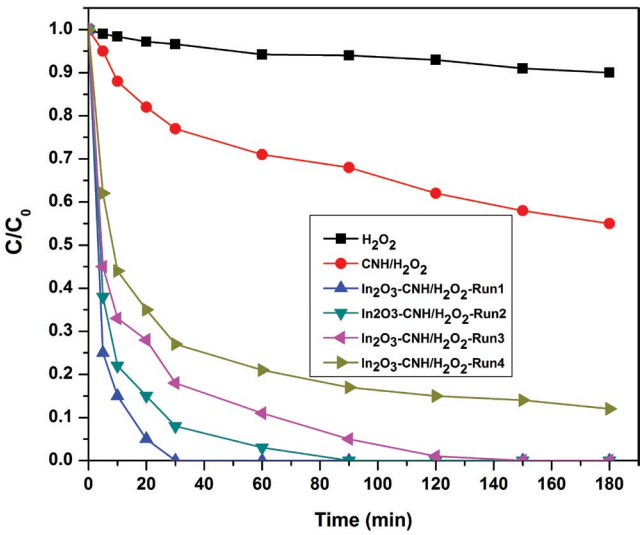

Fig. 9. Effect of catalyst performance and reusability cycles on the removal of MO dye (C_0 = 20 mg/L, catalyst dose = 1 g/L, T = 40°C, pH = 4 and $[H_2O_2]$ = 0.192 mol/L).

On the other hand, In_2O_3-CNH/H_2O_2 exhibited a superior degradation efficiency toward MO dye molecules where 100% (C/C_0 = 0) of dye is degraded quickly within 30 min. The higher catalytic performance of In_2O_3-CNH/H_2O_2 as compared to CHN is mainly attributed to the existence of reactive oxygen vacancies at the surface of In_2O_3 nanoparticles which promoted the decomposition rate of H_2O_2 to HO• radicals in large amounts. Therefore, the combination of In_2O_3 and CNH led to form a synergistic effect resulting in the development of active sites for the adsorption and catalytic oxidation processes toward the removal of MO dye molecules from aqueous solutions.

To estimate the stability of the prepared In_2O_3-CNH catalyst, four consecutive runs of CWO were employed and the results are shown in Fig. 9. During four successive runs, the degradation efficiency of In_2O_3-CNH was slightly decreased from 100% to 88% (C/C_0 = 0.12) at 180 min of the fourth run. Therefore, the reusability study confirms that the prepared nanohybrid catalyst displayed superior stability over three consecutive cycles (in which about 100 % removal of MO dye was obtained at 150 min).

4. Conclusions

In_2O_3 supported on a carbonaceous hybrid of carbon xerogel reinforced with GO as a heterogeneous catalyst for degradation of MO dye in the liquid phase was successfully obtained. It was found that the adsorption of MO dye is largely associated with the presence of In_2O_3 nanoparticles. The decomposition rate of MO dye was controlled by the temperature, pH and catalyst. Thus, the best catalytic oxidation conditions were attained at a temperature of 40°C, pH 4 with an initial MO concentration of 20 mg/L to degrade fully the dye at 30 min over In_2O_3-CNH. Results of reusability showed that the In_2O_3-CNH catalyst has an excellent catalytic performance during four cycles of CWO.

The enhanced adsorption capacity and catalytic efficiency of the In_2O_3-CNH catalyst are mainly attributed to the presence of In_2O_3 nanoparticles which acted as active adsorption and catalytic oxidation centers for removing MO dye from the aqueous solutions.

Acknowledgement

The authors gratefully acknowledge the financial support provided by the National Research Centre (NRC), Egypt, under the house-projects No. 11090201 and 11090313.

References

[1] T. Robinson, G. McMullan, R. Marchant, P. Nigam, Remediation of dyes in textile effluent: a critical review on current treatment technologies with a proposed alternative, Bioresour. Technol., 77 (2001) 247–255.
[2] G. Crini, Non-conventional low-cost adsorbents for dye removal: a review, Bioresour. Technol., 97 (2006) 1061–1085.
[3] M. Berrios, M.Á. Martín, A. Martín, Treatment of pollutants in wastewater: adsorption of methylene blue onto olive-based activated carbon, J. Ind. Eng. Chem., 18 (2012) 780–784.
[4] J.L. Faria, W. Wang, Carbon Materials in Photocatalysis, P. Serp, J.L. Figueiredo, Ed., Carbon Materials for Catalysis, John Wiley & Sons, Hoboken, NJ, 2009, pp. 481–506.
[5] W.H. Glaze, Drinking-water treatment with ozone, Environ. Sci. Technol., 21 (1987) 224–230.

[6] W.H. Glaze, J.-W. Kang, D.H. Chapin, The chemistry of water treatment processes involving ozone, hydrogen peroxide and ultraviolet radiation, Ozone Sci. Eng., 9 (1987) 335–352.
[7] Y. Deng, R.Z. Zhao, Advanced oxidation processes (AOPs) in wastewater treatment, Curr. Pollut. Rep., 1 (2015) 167–176.
[8] R.S. Ribeiro, N.A. Fathy, A.A. Attia, A.M.T. Silva, J.L. Faria, H.T. Gomes, Activated carbon xerogels for the removal of the anionic azo dyes Orange II and Chromotrope 2R by adsorption and catalytic wet peroxide oxidation, Chem. Eng. J., 195–196 (2012) 112–121.
[9] N.A. Fathy, S.E. El-Shafey, O.I. El-Shafey, W.S. Mohamed, Oxidative degradation of RB19 dye by a novel γ–MnO_2/MWCNT nanocomposite catalyst with H_2O_2, J. Environ. Chem. Eng., 1 (2013) 858–864.
[10] M.T. Pinho, A. Silva, N.A. Fathy, A.A. Attia, H.T. Gomes, J.L. Faria, Activated carbon xerogel-chitosan composite materials for catalytic wet peroxide oxidation under intensified process conditions, J. Environ. Chem. Eng., 3 (2015) 1243–1251.
[11] N.A. Fathy, S.M. El-Khouly, N.A. Hassan, Free- and Ni-doped carbon xerogels catalysts for wet peroxide oxidation of methyl orange, J. Water Process Eng., 16 (2017) 21–27.
[12] N.A. Fathy, S.E. El-Shafey, O.I. El-Shafey, Synthesis of a novel MnO_2@carbon nanotubes-graphene hybrid catalyst (MnO_2@CNT-G) for catalytic oxidation of basic red 18 dye (BR18), J. Water Process Eng., 17 (2017) 95–101.
[13] S.M. El-Khouly, G.M. Mohamed, N.A. Fathy, G.A. Fagal, Effect of nanosized CeO_2 or ZnO loading on adsorption and catalytic properties of activated carbon, Adsorpt. Sci. Technol., 35 (2017) 774–788.
[14] S.M. El-Khouly, N.A. Fathy, Multiwalled-carbon nanotubes supported amorphous Fe_2O_3- and Ag_2O-Fe_2O_3 as Fenton catalysts for degradation of maxilon red dye, Asia-Pac. J. Chem. Eng., 13 (2018) e2184, https://doi.org/10.1002/apj.2184.
[15] W.E. Rashwan, N.A. Fathy, S.M. Elkhouly, A novel catalyst of ceria-nanorods loaded on carbon xerogel for catalytic wet oxidation of methyl green dye, J. Taiwan Inst. Chem. Eng., 88 (2018) 234–242.
[16] N.A. Fathy, M.A. Shouman, R.M.M. Aboelenin, Nitrogen and phosphorous-doped porous carbon xerogels as metal-free catalysts for environmental catalytic peroxide oxidation of 4-nitrophenol, Asia-Pac. J. Chem. Eng., 11 (2016) 836–845.
[17] J. Lao, J. Huang, D. Wang, Z.F. Ren, Self-assembled In_2O_3 nanocrystal chains and nanowire networks, Adv. Mater., 16 (2004) 65–69.
[18] H. Zhu, N. Wang, L. Wang, K. Yao, X. Shen, In situ X-ray diffraction study of the phase transition of nanocrystalline $In(OH)_3$ to In_2O_3, Inorg. Mater., 41 (2005) 609–612.
[19] S. Kar, S. Chakrabarti, S. Chaudhuri, Morphology dependent field emission from In_2O_3 nanostructures, Nanotechnology, 17 (2006) 3058–3062.
[20] X. Chen, Z. Zhang, X. Zhang, J. Liu, Y. Qian, Single-source approach to the synthesis of In_2S_3 and In_2O_3 crystallites and their optical properties, Chem. Phys. Lett., 407 (2005) 482–486.
[21] M. Ivanovskaya, A. Gurlo, P. Bogdanov, Mechanism of O_3 and NO_2 detection and selectivity of In_2O_3 sensors, Sens. Actuators, B, 77 (2001) 264–267.
[22] D.V. Shinde, D.Y. Ahn, V.V. Jadhav, D.Y. Lee, N.K. Shrestha, J.K. Lee, H.Y. Lee, R.S. Mane, S.-H. Han, A coordination chemistry approach for shape controlled synthesis of indium oxide nanostructures and their photoelectrochemical properties, J. Mater. Chem. A, 2 (2014) 5490–5498
[23] Q. Tang, W. Zhou, W. Zhang, S. Ou, K. Jiang, W. Yu, Y. Qian, Size-controllable growth of single crystal $In(OH)_3$ and In_2O_3 nanocubes, Cryst. Growth Des., 5 (2005) 147–150.
[24] Y. Zhao, A.Z. Wu, H. Dang, Synthesis and characterization of single-crystalline In_2O_3 nanocrystals via solution dispersion, Langmuir, 6 (2004) 27–29.
[25] R. Sharma, R.S. Mane, S.K. Min, S.H. Han, Optimization of growth of In_2O_3 nano-spheres thin films by electrodeposition for dye-sensitized solar cells, J. Alloys Compd., 479 (2009) 840–843.
[26] Z. Li, P. Zhang, T. Shao, J. Wang, L. Jin, X. Li, Different nanostructured In_2O_3 for photocatalytic decomposition of perfluorooctanoic acid (PFOA), J. Hazard. Mater., 260 (2013) 40–46.
[27] L. Zhang, F.B. Gu, Z.H. Wang, D.M. Han, G.S. Guo, Preparation of In_2O_3/MWCNTs nanocomposites and their gas-sensing property to ethanol, Key Eng. Mater., 562 (2013) 543–548.
[28] Z. Li, P. Zhang, J. Li, T. Shao, L. Jin, Synthesis of In_2O_3-graphene composites and their photocatalytic performance towards perfluorooctanoic acid decomposition, J. Photochem. Photobiol., A, 271 (2013) 111–116.
[29] L. Zhao, W. Yue, Y. Ren, Synthesis of graphene-encapsulated mesoporous In_2O_3 with different particle size for high-performance lithium storage, Electrochim. Acta, 116 (2014) 31–38.
[30] S. Qin, D. Liu, W. Lei, Y. Chen, Synthesis of an indium oxide nanoparticles embedded graphene three-dimensional architecture for enhanced lithium-ion storage, J. Mater. Chem. A, 3 (2015)18238–18243
[31] J. Liu, S. Li, B. Zhang, Y. Wang, Y. Gao, X. Liang, Y. Wang, G. Lu, Flower-like In_2O_3 modified by reduced graphene oxide sheets serving as a highly sensitive gas sensor for trace NO_2 detection, J. Colloid Interface Sci., 504 (2017) 206–213
[32] L.-Y. Chen, W.-D. Zhang, In_2O_3/g-C_3N_4 composite photocatalysts with enhanced visible light driven activity, Appl. Surf. Sci., 301 (2014) 428–435.
[33] H. Zhao, H. Yin, X.-X. Yu, W. Zhang, C. Li, M.-Q. Zhu, In_2O_3 nanoparticles/carbon fiber hybrid mat as free-standing anode for lithium-ion batteries with enhanced electrochemical performance, J. Alloys Compd., 735 (2018) 319–326.
[34] K. Guo, H. Song, X. Chen, X. Du, L. Zhong, Graphene oxide as an anti-shrinkage additive for resorcinol–formaldehyde composite aerogels, Phys. Chem. Chem. Phys., 16 (2014) 11603–11608.
[35] M.A. Worsley, P.J. Pauzauskie, T.Y. Olson, J. Biener, J.H. Satcher Jr., T.F. Baumann, Synthesis of graphene aerogel with high electrical conductivity, J. Am. Chem. Soc., 132 (2010) 14067–14069.
[36] F. Meng, X. Zhang, B. Xu, S. Yue, H. Guo, Y. Luo, Alkali-treated graphene oxide as a solid base catalyst: synthesis and electrochemical capacitance of graphene/carbon composite aerogels, J. Mater. Chem., 21 (2011) 18537–18539.
[37] Q. Lei, H. Song, X. Chen, M. Li, A. Li, B. Tang, D. Zhou, Effects of graphene oxide addition on the synthesis and supercapacitor performance of carbon aerogel particles, RSC Adv., 6 (2016) 40683–40690.
[38] R.W. Pekala, Organic aerogels from the polycondensation of resorcinol with formaldehyde, J. Mater. Sci., 24 (1989) 3221–3227.
[39] B.S. Girgis, A.A. Attia, N.A. Fathy, Potential of nano-carbon xerogels in the remediation of dye-contaminated water discharges, Desalination, 265 (2011) 169–176.
[40] D.C. Marcano, D.V. Kosynkin, J.M. Berlin, A. Sinitskii, Z. Sun, A. Slesarev, L.B. Alemany, W. Lu, J.M. Tour, Improved synthesis of graphene oxide, ACS Nano, 4 (2010) 4806–4814.
[41] K.P. Annamalai, L. Liu, Y. Tao, Highly nanoporous nickel cobaltite hexagonal nanostructure-graphene composites for the next generation energy storage/conversion devices, Adv. Mater. Interfaces, 4 (2017), doi.org/10.1002/admi.201700219.
[42] H.K. Farag, M.A. Marzouk, Preparation and characterization of nanostructured nickel oxide and its influence on the optical properties of sodium zinc borate glasses, J. Mater. Sci. - Mater. Electron., 28 (2017) 15480–15487.
[43] H.K. Farag, A.M. El Shamy, E.M. Sherif, S.Z. El Abedin, Sonochemical synthesis of nanostructured ZnO/Ag composites in an ionic liquid, Z. Phys. Chem., 203 (2016) 1733–1744.
[44] I. Langmuir, The adsorption of gases on plane surfaces of glass, mica and platinum, J. Am. Chem. Soc., 40 (1918) 1361–1403.
[45] H.M.F. Freundlich, Over the adsorption in solution, J. Phys. Chem., 57 (1906) 385–470.
[46] M.I. Temkin, V. Pyzhev, Kinetic of ammonia synthesis on promoted iron catalyst, Acta Phys. Chim. Sin. URSS, 12 (1940) 327–356.
[47] N.A. Fathy, R.R. Abd El-Latif, R.M.M. Aboelenin, L.B. Khalil, Green reduction of oxidized graphite to reduced graphene oxide using *Zygophyllum album* L.f.: comparative adsorption

studies on *p*-nitrophenol, Recent Innovations Chem. Eng., 8 (2015) 87–102.
[48] P. Bautista, A.F. Mohedano, N. Menendez, J.A. Casas, J.J. Rodriguez, Catalytic wet peroxide oxidation of cosmetic wastewaters with Fe-bearing catalysts, Catal. Today, 151 (2010) 148–152.
[49] M. Arshadi, A.R. Faraji, M.J. Amiri, Synthesis and adsorption characteristics of an heterogenized manganese nanoadsorbent towards methyl orange, J. Colloid Interface Sci., 440 (2015) 189–197.
[50] J. Herney-Ramirez, M.A. Vicente, L.M. Madeira, Heterogeneous photo-Fenton oxidation with pillared clay-based catalysts for wastewater treatment: a review, Appl. Catal., B, 98 (2010) 10–26.
[51] S. Zhang, D. Wang, L. Zhou, X. Zhang, P. Fan, X. Quan, Intensified internal electrolysis for degradation of methylene blue as model compound induced by a novel hybrid material: multi-walled carbon nanotubes immobilized on zero-valent iron plates (Fe^0-CNTs), Chem. Eng. J., 217 (2013) 99–107.
[52] M. Arshadia, M.K. Abdolmaleki, F. Mousavinia, A. Khalafi-Nezhad, H. Firouzabadi, A. Gil, Degradation of methyl orange by heterogeneous Fenton-like oxidation on a nano-organometallic compound in the presence of multi-walled carbon nanotubes, Chem. Eng. Res. Des., 112 (2016) 113–121.